# Superdense hexagonal BP and AlP with quartz topology: Crystal chemistry and DFT study

Vladimir Solozhenko, Samir Matar

▶ **To cite this version:**

Vladimir Solozhenko, Samir Matar. Superdense hexagonal BP and AlP with quartz topology: Crystal chemistry and DFT study. Crystals, 2023, 13 (12), pp.1622. 10.3390/cryst13121622 . hal-04301103

**HAL Id: hal-04301103**
**https://hal.science/hal-04301103v1**

Submitted on 22 Nov 2023

**HAL** is a multi-disciplinary open access archive for the deposit and dissemination of scientific research documents, whether they are published or not. The documents may come from teaching and research institutions in France or abroad, or from public or private research centers.

L'archive ouverte pluridisciplinaire **HAL**, est destinée au dépôt et à la diffusion de documents scientifiques de niveau recherche, publiés ou non, émanant des établissements d'enseignement et de recherche français ou étrangers, des laboratoires publics ou privés.

# Superdense hexagonal BP and AlP with quartz topology: Crystal chemistry and DFT study

Vladimir L. Solozhenko[1,*] and Samir F. Matar[2]

[1] LSPM–CNRS, Université Sorbonne Paris Nord, 93430 Villetaneuse, France
https://orcid.org/0000-0002-0881-9761

[2] Lebanese German University, Jounieh, P.O. Box 206, Lebanon
https://orcid.org/0000-0001-5419-358X

## Abstract

The superdense hexagonal phosphides BP and AlP, whose structures are formed by distorted tetrahedra and characterized by quartz-derived (**qtz**) topology, were predicted from crystal chemistry and first principles as potential high-pressure phases. From full geometry structure relaxations and ground state energies calculations based on quantum density functional theory (DFT), **qtz** BP and AlP were found to be less cohesive than the corresponding cubic zinc-blende (*zb*) phases with diamond-like (**dia**) topology, but were confirmed to be mechanically (elastic constants) and dynamically (phonons) stable. From the energy-volume equations of state, **qtz** phases were found to be energetically favorable at small volumes, with *zb*-to-**qtz** transition pressures of 144 GPa for BP and 28 GPa for AlP. According to the electronic band structures and the site projected density of states, both phosphides exhibit larger band gaps of the zinc-blende phases compared to the **qtz** phases; the smaller values for the latter result from the smaller volumes per formula unit, leading to an increased covalence.

***Keywords***: BP; AlP; topology; DFT; elastic constants; equation-of-state, phonons

[*] Corresponding author (e-mail: vladimir.solozhenko@univ-paris13.fr)

## 1. Introduction

III-V compound semiconductors composed of $III^A$-group electropositive elements (B, Al, Ga, In) combined with $V^A$-group electronegative elements (N, P, As, Sb) have long been considered a promising material basis for a number of well-established commercial technologies, as well as for new advanced classes of electronic and optoelectronic devices [1-4]. Examples include heterostructure and high-electron-mobility bipolar transistors, light-emitting diodes, diode lasers, photodetectors, and electro-optic modulators. The physical properties of the constituent materials are critical to the operating characteristics of these devices.

Under normal conditions, the majority of III-V semiconductor compounds crystallize in the cubic zinc-blende (*zb*) structure (space group *F*-43*m*, No. 216), and these compounds can be considered as a single series in which there is a gradual change of chemical bonding from the covalent type to the iono-covalent type, while the bonding energy is virtually determined by the first tetrahedral coordination sphere.

For III-V compounds of light elements, while *zb*-BN is characterized by a large band gap ($E_g$ = 6.36(3) eV [5]), a value three times smaller is reported for *zb*-BP: $E_g \approx 2.1$ eV [6]. In fact, boron nitride is polar covalent with significant charge transfer from B to N as opposed to BP where less charge transfer is expected. The difference in behavior has a chemical origin derived from the electronegativity ($\chi$) values according to Pauling: $\chi$B= 2.04; $\chi$N = 3.04 with $\Delta\chi$(BN) = 1. Conversely, with $\chi$P = 2.19, $\Delta\chi$(BP) = 0.15, and BP is considered as a covalent semiconductor (cf. [7]). As for Al belonging to the 2nd period, $\chi$Al = 1.50, and for AlP $\Delta\chi_{(Al\text{-}P)}$ = |0.69|, i.e. more than four times larger than in the case of BP.

Recently, we found a significant densification (with increased hardness) for BN and SiC when adopting a quartz-derived structure, i.e., **qtz** topology [8]. The aim of the present work is to extend the model approach to equiatomic monophosphides of $III^A$-group elements and to consider the possibility of their phase transitions at high pressure into superdense quartz-based hexagonal phases. Such high-pressure structures have been identified for zinc chalcogenides in addition to the cubic zinc-blende polymorphs adopted by the other II-VI compounds [9].

As in previous works [7,8], our investigations are based on calculations of energies, structures, and derived properties within the density functional theory (DFT) quantum mechanics framework [10,11]. Specifically, superdense **qtz** BP and AlP were found to be cohesive, albeit with smaller magnitudes than known for zinc-blende BP and AlP with **dia** topology (*vide infra,* section 3.1), and were identified as stable both mechanically (elastic constants) and dynamically (phonon band structures). From the establishment of the respective equations of states (EOS), the trends of *zb*-BP and *zb*-AlP transformations to **qtz** high-pressure forms maintaining a tetrahedral coordination have been identified. The electronic band structures of the new **qtz** phases show reduced band gaps compared to zinc-blende polymorphs.

## 2. Computational methodology

The identification of the ground state structures corresponding to the energy minima and prediction of their mechanical and dynamical properties were carried out by DFT-based calculations using the Vienna Ab initio Simulation Package (VASP) code [12,13] and the projector augmented wave (PAW) method [13,14] for the atomic potentials. Exchange correlation (XC) effects were considered using the generalized gradient functional approximation (GGA) [15]. The relaxation of the atoms to the ground state structures was performed with the conjugate gradient algorithm according to Press *et al*. [16]. The Blöchl tetrahedron method [17] with corrections according to the Methfessel and Paxton scheme [18] was used for geometry optimization and energy calculations, respectively. Brillouin zone (BZ) integrals were approximated by a special **k**-point sampling according to Monkhorst and Pack [19]. Structural parameters were optimized until atomic forces were below 0.02 eV/Å and all stress components were < 0.003 eV/Å$^3$. The calculations were converged at an energy cutoff of 400 eV for the plane-wave basis set in terms of the **k**-point integration in the reciprocal space from $k_x(6)\times k_y(6)\times k_z(4)$ up to $k_x(12)\times k_y(12)\times k_z(8)$ for the final convergence and relaxation to zero strains. In the post-processing of the ground state electronic structures, the charge density projections were operated on the lattice sites.

The mechanical stability and hardness were obtained from the elastic constants calculations. The analysis of the elastic tensors was carried out using the ELATE software [20], which provides the bulk ($B$), shear ($G$) and Young's ($E$) moduli along different averaging methods; Voigt's method [16] was chosen here. Vickers hardness ($H_V$) from elastic properties was evaluated using the empirical Mazhnik-Oganov model [21].

The dynamic stabilities of the considered phases were confirmed from the positive phonon magnitudes. The corresponding phonon band structures were obtained from a high resolution of the Brillouin zone according to Togo and Tanaka [22]. The electronic band structures were obtained using the all-electron DFT-based ASW method [23] and GGA XC functional [15]. The program VESTA (Visualization for Electronic and STructural Analysis) [24] was used to visualize the crystal structures and charge densities.

## 3. Results and Discussion

### *3.1 Crystal chemistry*

With the aim of classifying structures into families, a topological representation for crystal types has been proposed using the TopCryst system [25]. Cubic diamond has **dia** topology and its rare hexagonal form called "lonsdaleite" has **lon** topology. These two topological types are characteristic of a large number of crystal systems. For example, zinc-blende phases have *dia* topology and wurtzite phases have **lon** topology. Recently, a hexagonal tricarbon $C_3$ allotrope was claimed from *ab initio* studies to be superdense and superhard with an assigned **qtz** topology [26]. Later, we

proposed **qtz** $C_6$, which is characterized by an ultrahardness comparable (or even superior) to that of diamond [27]. For the sake of completeness, we note that the **qtz** topology is also adopted by trigonal binary phases [8].

The III-V compounds crystallize

- either in tetrahedral coordination as zinc-blende ZnS (space group *F*-43*m*, No. 216; **dia** topology) and wurtzite ZnO (space group $P6_3mc$, No. 186; **lon** topology);
- or in octahedral coordination as rocksalt NaCl (space group *Fm*-3*m*, No.°225; **pcu** topology) and NiAs (space group $P6_3/mmc$, No. 194; **seh** topology).

Knowing that a tetrahedral void is larger than an octahedral void, one might expect denser NaCl and NiAs-type structures to prevail at high pressures. However, an interesting feature of the topology of **qtz** systems, i.e. very high density, is used in the present work to propose new hypothetical high-pressure phases with tetrahedral topology for the well-known III-V phosphides, BP and AlP, based on crystal chemistry and DFT studies. Gallium and indium phosphides are not considered here due to their dynamic instability (see section 3.5 for details).

The ground state structures of zinc-blende BP and AlP belong to the high symmetry space group *F*-43*m* where B/Al atoms occupy the 4a position and P atoms occupy the 4c position. The corresponding structures presented in Fig. 1 show a perfectly regular arrangement of tetrahedra with the characteristic tetrahedral angle of ∠109.47°. The calculated structure parameters are very close to the experimental values [28,29] (cf. Table 1).

The alternative description of the **qtz** $C_6$ structure (space group $P6_522$, No. 179 with unique (6a) sites [27]) is possible in space group $P6_422$, No. 181 with two distinct Wyckoff positions, namely (3c) and (3d), as shown in Table 1. Such a configuration corresponds to the binary equiatomic phosphides BP and AlP. The lattice parameters of the ground state structures are given in Table 1. The corresponding crystal structures are shown in Fig. 1 with ball-and-stick and tetrahedral representations, the latter featuring corner-sharing irregular tetrahedra (*vide infra*). The atoms occupy the Wyckoff positions (3c) ½, 0, 0 and (3d) ½, 0, ½. Differences are observed in the volumes (total and atom-averaged) and the interatomic distances, which increase due to the large increase of the atomic radius from B to Al: 0.83 Å versus 1.83 Å; r(P)=1.10 Å. Looking at the angles related to the constituent tetrahedra, they differ significantly from the regular tetrahedral type (∠109.47°), thus showing the specificity of the **qtz** topology. From Table 1, which shows the energy per formula unit (FU), the **qtz** structures are cohesive and have higher energies than the zinc-blende ones, known as the ground state structures at normal conditions. In terms of volume per FU, smaller volumes characterize the **qtz** phases suggesting possible transitions at high pressures (*vide infra*).

### *3.2 Projections of the charge densities*

For a qualitative assessment, Fig. 2 shows the projected charge densities (yellow volumes) that are found to be centered on the electronegative element P with a shape difference between BP and AlP.

In BP, a tetrahedral shape of the charge density on P is observed with a skew towards B. In contrast, in AlP, a charge centered on P is observed.

Such observations were further quantified by treating the respective charge density output files using the AIM (atoms in molecules theory) approach developed by Bader [30]. The charge density in a chemical compound reaches a minimum between atoms thus defining a region that separates atoms from each other. The results of the charge transfer δ are: δ(BP) = 0.30 and δ(AlPN) = 2.60, indicating a stronger trend from covalent to ionic character of AlP, which can be explained by the electronegativity χ difference between the constituent atoms (see Introduction).

### *3.3 Mechanical properties*

The analysis of the mechanical properties of the new **qtz** phosphides has been carried out by calculating the elastic tensor through finite distortions of the lattice. The calculated sets of elastic constants $C_{ij}$ (i and j correspond to directions) for cubic zinc-blende and hexagonal **qtz** and NiAs-type phases are given in Table 2. For comparison, the values obtained for **qtz** $C_6$ [27] were added. All $C_{ij}$ values are positive, suggesting mechanically stable phases. **qtz** $C_6$ has the largest $C_{ij}$ values, while **qtz** BP and **qtz** AlP have significantly smaller elastic constants. The new phases are fully described by the bulk (*B*), shear (*G*) and Young's (*E*) moduli obtained by Voight's averaging [31] of the elastic constants using ELATE software [20]. The last three columns of Table 2 show the elastic moduli, with values that follow the trends observed for $C_{ij}$. It is evident that AlP is significantly more compressible than BP, both in the case of the cubic (*zb*) and the hexagonal (**qtz** and NiAs-type) phases.

The Vickers hardness ($H_V$) of the new phosphides has been predicted using two contemporary models: the thermodynamic (T) model [32], which is based on thermodynamic properties and crystal structure, and shows perfect agreement with available experimental data [33-35], and the empirical Mazhnik-Oganov (MO) model [21], which is based on elastic properties. The results are summarized in Table 3. Both **qtz** and zinc-blende BP are (super)hard phases, while the hardness of all AlP polymorphs is three times lower.

### *3.4 Equations of state and possible high-pressure phase transitions*

When considering different crystal structures of a solid, comparative energy trends can be determined from their equations of state (EOS). This was done from a series of calculations of the total energy as a function of volume for cubic and hexagonal phases of BP and AlP. The resulting E(V) curves, shown in Fig. 3, were fitted to the third-order Birch equations of state [36]:

$$E(\mathrm{V}) = E_0(\mathrm{V}_0) + (9/8)\cdot \mathrm{V}_0 B_0[([(\mathrm{V}_0)/\mathrm{V}])^{2/3} - 1]^2 + (9/16)\cdot B_0(B_0' - 4)\mathrm{V}_0[([(\mathrm{V}_0)/\mathrm{V}])^{2/3} - 1]^3,$$

where $E_0$, $V_0$, $B_0$ and $B_0'$ are the equilibrium energy, volume, bulk modulus and its first pressure derivative, respectively. (see Table 4). In the case of boron phosphide (Fig. 3a), the intersection of E(V) curves of zinc-blende and **qtz** phases is observed at V/FU = 15.6 Å, which for *zb*-BP is equivalent to a reduced volume of 0.67. The corresponding pressure can be calculated by the Murnaghan equation [39]

$$p = B_0/B_0' [(V_0)/V])^{B_0'} - 1]$$

using the experimental values of $B_0$ and $B_0'$ (Table 4), and is equal to 144 GPa. Thus, it can be assumed that the phase transformation of *zb*-BP into **qtz** BP can occur at pressures not lower than 144 GPa, which is in agreement with the experimental data on the absence of room-temperature phase transitions of *zb*-BP up to 110 GPa [40].

In the case of aluminum phosphide (Fig. 3b), the intersection of the E(V) curves of *zb*-AlP and **qtz** AlP is observed at V/FU = 33.84 Å ($V/V_0$ = 0.81 for *zb*-AlP). The corresponding pressure calculated using the experimental $B_0$ and $B_0'$ values of *zb*-AlP (Table 4) is equal to 28 GPa, i.e. **qtz** AlP formation could be expected at higher pressures. However, at room temperature, the phase transformation of *zb*-AlP into a high-pressure phase with NiAs-type structure, which is energetically favorable over the whole pressure range, is observed already at about 10 GPa [41]. Thus, the formation of **qtz** AlP at sufficiently high (> 28 GPa) pressures can only be possible as a result of alternative metastable behavior under far-from-equilibrium conditions (shock compression, etc.).

### *3.5 Dynamic and thermodynamic properties from the phonons*

An important criterion for phase dynamic stability can be obtained from the phonon properties. Phonons are vibrational quanta whose energy is quantized using the Planck constant h in its reduced form ħ (ħ = h/2π), which gives the phonons energy: E = ħω (frequency: ω). The phonon band structures (red lines) obtained following the protocol presented in section 2 are shown in Fig. 4. The horizontal direction shows the main directions of the hexagonal center of the Brillouin zone, while the vertical direction shows the frequencies ω, given in units of terahertz (THz). The absence of negative frequencies indicates dynamically stable systems. The band structure includes 3N bands with 3N-3 optical modes found at higher energies than three acoustic modes starting from zero energy (ω = 0) at the Γ point, the center of the BZ, up to a few terahertz. They correspond to the lattice rigid translation modes of the crystal (two transverse and one longitudinal). While the different panels show positive frequency (ω) magnitudes, a slightly negative phonon curve is observed along Γ-A (vertical direction), around Γ, center of the BZ. This indicates a slight instability of the longitudinal acoustic mode, which may result from the almost double volume of AlP (37.08 $Å^3$/FU) compared to BP (21.60 $Å^3$/FU). The resulting openness of the AlP structure is consistent with the structurally dense **qtz** topology. This observation explains the reason why GaP and InP, characterized by large atomic radii of Ga (1.35 Å) and In (1.47 Å), could not be dynamically stabilized in **qtz** topology as it follows from our preliminary study (Fig. 4 *e*,*f*).

The thermodynamic properties of the new **qtz** phases were calculated from the phonon frequencies using the statistical thermodynamic approach [42] on a high-precision sampling mesh in the Brillouin zone. The temperature dependencies of the heat capacity at constant volume ($C_v$) and entropy (S) of **qtz** BP and **qtz** AlP are shown in Fig. 5 in comparison with experimental $C_p$ data for *zb*-BP [43,44] and *zb*-AlP [45]. It is easy to see that the heat capacity of *zb*-BP is higher than that of **qtz** BP in the whole temperature range studied, while the heat capacity of *zb*-AlP in the range 300-1000 K practically coincides with the heat capacity of **qtz** AlP. Experimental data on the low-temperature heat capacity of *zb*-AlP are not available in the literature.

### *3.6 Electronic band structures*

Using the crystal parameters in Table 1, the electronic band structures were obtained using the all-electrons DFT-based augmented spherical method (ASW) [23] and are shown in Fig. 6. The bands (blue lines) develop along the major directions of the hexagonal Brillouin zones. The zero energy along the vertical axis is considered with respect to $E_V$, at the top of the filled valence band (VB), separated from the empty conduction band (CB) by a band gap. For both phosphides, the zinc-blende phase has a larger band gap compared to the **qtz** phase, the smaller magnitude for the latter resulting from the smaller volume per FU leading to increased covalence.

The band structures are mirrored by the site projected densities of states (DOS) shown in the right part of Fig. 6. As a general feature, the P(DOS) show higher intensity than the B(DOS) and Al(DOS) due to the lower electronegativities of boron and aluminum compared to phosphorus, as discussed above. The Fermi level is represented by a vertical line at 0 along the horizontal energy axis, while the vertical axis corresponds to the DOS expressed in $eV^{-1}$ units, translating the number of states per unit energy. The valence band (VB) is wider in BP than in AlP with the characteristics of a small separation between s-prevailing states from -16 to -10 eV and the p-prevailing states from -9 eV up to $E_V$ (top of the VB) in BP, and a larger separation for s-states from -12 to -9 eV and p-states from -6 up to $E_V$ in AlP. Such a feature can be related to the larger interatomic distances in AlP vs. BP.

## 4. Conclusions

Based on crystal chemistry and DFT calculations, superdense hexagonal ($P6_422$) BP and AlP were proposed as potential high-pressure phases with quartz-derived topology. They were found to be cohesive, albeit at higher energies than the corresponding cubic zinc-blende phases, stable at ambient pressure. **qtz** BP and AlP tend to dominate at low volumes, and the threshold pressures of the cubic-to-hexagonal phase transition are 144 and 28 GPa, respectively. At the local level, the transition mechanism is related to the distortion of the *BP4* / *AlP4* tetrahedra that characterizes the **qtz** topology. Smaller volumes per formula unit lead to increased covalency of both **qtz** phosphides, resulting in lower band gap values compared to the corresponding zinc-blende phases.

## References


[1] Quillec, M. (Ed.) *Materials for Optoelectronics*. Kluwer Academic: Boston, USA, 1996

[2] Levinshtein, M.; Rumyantsev, S.; Shur, M. *Handbook Series on Semiconductor Parameters.* vol. 1. World Scientific: Singapore, 1999.

[3] Vurgaftman, I.; Meyer, J.R.; Ram-Mohan L.R. Band parameters for III-V compound semiconductors and their alloys. *J. Appl. Phys.* **2001**, *89*, 5815-5875.

[4] Adachi, S. *Physical Properties of III-V Semiconductor Compounds.* Wiley-VCH: Weinheim, 2004.

[5] Evans, D.A.; McGlynn, A.G.; Towlson, B.M.; Gunn, M.; Jones, D.; Jenkins, T.E.; Winter, R; Poolton, N.R.J. Determination of the optical band-gap energy of cubic and hexagonal boron nitride using luminescence excitation spectroscopy. *J. Phys. Condens. Matter* **2008**, *20*, 075233.

[6] Agui, A.; Shin, S.; Kumashiro, Y. Electronic structure of BP studied by resonant soft X-ray emission spectroscopy. *J. Phys. Soc. Jpn.* **1999**, *68*, 166-169.

[7] Solozhenko, V.L.; Matar, S.F. Polymorphism of boron phosphide: Theoretical and experimental assessments. *J. Mater. Chem. C* **2022**, *10*, 3937-3943.

[8] Matar, S.F.; Solozhenko, V.L. Ultrahigh-density superhard hexagonal BN and SiC with quartz topology from crystal chemistry and first principles. *Crystals* **2023**, *13*, 1498.

[9] McMahon, M.I.; Nelmes, R.J.; Wright, N.G.; Allan, D.R. Crystal structure studies of II-VI semiconductors using angle-dispersive diffraction techniques with an image-plate detector. *AIP Conf. Proc.* **1994**, *309*, 633-636.

[10] Hohenberg, P.; Kohn, W. Inhomogeneous electron gas. *Phys. Rev. B* **1964**, *136*, 864-871.

[11] Kohn, W.; Sham, L.J. Self-consistent equations including exchange and correlation effects. *Phys. Rev. A* **1965**, *140*, 1133-1138.

[12] Kresse, G.; Furthmüller, J. Efficient iterative schemes for ab initio total-energy calculations using a plane-wave basis set. *Phys. Rev. B* **1996**, *54*, 11169.

[13] Kresse, G.; Joubert, J. From ultrasoft pseudopotentials to the projector augmented wave. *Phys. Rev. B* **1999**, *59*, 1758-1775.

[14] Blöchl, P.E. Projector augmented wave method. *Phys. Rev. B* **1994**, *50*, 17953-17979.

[15] Perdew, J.; Burke, K.; Ernzerhof, M. The Generalized Gradient Approximation made simple. *Phys. Rev. Lett.* **1996**, *77*, 3865-3868.

[16] Press, W.H.; Flannery, B.P.; Teukolsky, S.A.; Vetterling, W.T. Numerical Recipes, 2nd ed.; Cambridge University Press: New York, USA, 1986.

[17] Blöchl, P.; Jepsen, O.; Anderson, O. Improved tetrahedron method for Brillouin-zone integrations. *Phys. Rev. B* **1994**, *49*, 16223-16233.

[18] Methfessel, M.; Paxton, A.T. High-precision sampling for Brillouin-zone integration in metals. *Phys. Rev. B* **1989**, *40*, 3616–3621.

[19] Monkhorst, H.J.; Pack, J.D. Special k-points for Brillouin Zone integration. *Phys. Rev. B* **1976**, *13*, 5188–5192.

[20] Gaillac, R.; Pullumbi, P.; Coudert, F.X. ELATE: an open-source online application for analysis and visualization of elastic tensors. *J. Phys.: Condens. Matter* **2016**, *28*, 275201.

[21] Mazhnik, E.; Oganov, A.R. A model of hardness and fracture toughness of solids. *J. Appl. Phys.* **2019**, *126*, 125109.

[22] Togo, A.; Tanaka, I. First principles phonon calculations in materials science, *Scr. Mater.* **2015**, *108*, 1-5.

[23] Eyert, V. Basic notions and applications of the augmented spherical wave method. *Int. J. Quantum Chem.* **2000**, *77*, 1007-1031.

[24] Momma, K.; Izumi, F. VESTA3 for three-dimensional visualization of crystal, volumetric and morphology data. *J. Appl. Crystallogr.* **2011**, *44*, 1272-1276.

[25] Shevchenko, A.P.; Shabalin, A.A.; Karpukhin, I.Yu.; Blatov, V.A. Topological representations of crystal structures: generation, analysis and implementation in the *TopCryst* system. *Sci Technol Adv Mat.* **2022**, *2*, 250-265.

[26] Luo, B.; Wu, L.; Zhang, Z.; Li, G.; Tian, E. A triatomic carbon and derived pentacarbides with superstrong mechanical properties. *iScience* **2022**, *25*, 104712.

[27] Matar, S.F.; Solozhenko, V.L. First principles search for novel ultrahard high-density carbon allotropes: hexagonal $C_6$, $C_9$ and $C_{12}$. *J. Superhard Mater.* **2023**, *45*, 239-248.

[28] Rundqvist, S. Crystal structure of boron phosphide BP. In: *Congres International de chimie pure et applique*. **1958**, *16*, 539-540.

[29] Richman, D. Vapor phase growth and properties of aluminum phosphide. *J. Electrochem. Soc.* **1968**, *115*, 945-947.

[30] Bader, R.F.W. A quantum theory of molecular structure and its applications. *Chem. Rev.* **1991**, *91*, 893-928.

[31] Voigt, W. Über die Beziehung zwischen den beiden Elasticitätsconstanten isotroper Körper. *Annal. Phys.* **1889**, *274*, 573-587.

[32] Mukhanov, V.A.; Kurakevych, O.O.; Solozhenko, V.L. The interrelation between hardness and compressibility of substances and their structure and thermodynamic properties. *J. Superhard Mater.* **2008**, *30*, 368-378.

[33] Solozhenko, V.L.; Bushlya, V. Mechanical properties of boron phosphides. *J. Superhard Mater.* **2019**, *41*, 84-89.

[34] Solozhenko, V.L. Hardness of new boron-rich chalcogenides $B_{12}S$ and $B_{12}Se$. *J. Superhard Mater.* **2021**, *43*, 375-377.

[35] Solozhenko, V.L. On hardness of boron subarsenide $B_{12}As_2$. *J. Superhard Mater.* **2022**, *44*, 377-378.

[36] Birch, F. Finite strain isotherm and velocities for single-crystal and polycrystalline NaCl at high pressures and 300 K. *J. Geophys. Res*. **1978**, *83*, 1257-1268.

[37] Solozhenko, V.L.; Kurakevych, O.O.; Le Godec, Y.; Kurnosov, A.V.; Oganov, A.R. Boron phosphide under pressure: in situ study by Raman scattering and X-ray diffraction. *J. Appl. Phys.* **2014**, *116*, 033501.

[38] Wiley, J.D. in *Semiconductors and Semimetals*, vol. 10 (eds. Willardson, R.K.; Beer, A.C.) Academic Press: New York, 1975.

[39] Murnaghan F.D. The compressibility of media under extreme pressures. *Proc. Nation. Acad. Sci. USA* **1944**, *30*, 244-247.

[40] Xia, H.; Xia, Q.; Ruoff, A.L. BP at megabar pressures and its equation of state to 110 GPa. *J. Appl. Phys*. **1993**, *74*, 1660-1662.

[41] Greene, R.G.; Luo, H.; Ruoff, A.L. High pressure study of AIP: Transformation to a metallic NiAs phase. *J. Appl. Phys*. **1994**, *76*, 7296-7299

[42] Dove, M.T. Introduction to lattice dynamics. Cambridge University Press: New York, 1993.

[43] Ohsawa, J.; Nishinaga,T.; Uchiyama, S. Measurement of specific heat of boron monophosphide by AC calorimetry. *Jpn. J. Appl. Phys.* **1978**, *17*, 1059-1065.

[44] Koshchenko, V.I.; Grinberg, Ya.Kh.; Demidenko, A.F. Thermodynamic properties of AlN (5-2700 K), GaP (5-1500 K) and BP (5-800 K). *Izv. Akad. Nauk SSSR, Neorg. Mater.* **1984**, *20*, 1787-1790 (in Russian).

[45] Neviak, S.O; Sandulova, A.V. Thermodynamic characteristics of aluminum phosphide. *Izv. Akad. Nauk SSSR, Neorg. Mater.* **1974**, *10*, 146-147 (in Russian).

Table 1. Crystal structure parameters of BP and AlP polymorphs.

| | *zb*-BP (Z = 4)<br>*F*-43*m* (No. 216) | **qtz** BP (Z = 3)<br>$P6_422$ (No. 181) | *zb*-AlP (Z = 4)<br>*F*-43*m* (No. 216) | **qtz** AlP (Z = 3)<br>$P6_422$ (No. 181) |
|---|---|---|---|---|
| *a*, Å | 4.541 (4.538 [28]) | 3.274 | 5.501 (5.463 [29]) | 3.854 |
| *c*, Å | – | 6.983 | – | 8.658 |
| $V_{cell}$, Å$^3$ | 93.64 | 64.82 | 166.50 | 111.25 |
| V/FU, Å$^3$ | 23.41 | 21.61<br>$\Delta V^{zb\text{-}qtz}$ /FU = 1.80 | 41.63 | 37.08<br>$\Delta V^{zb\text{-}qtz}$ /FU = 4.55 |
| Shortest bond, Å | 1.97 | 2.00 | 2.38 | 2.40 |
| Angles (deg.) | 109.47 | 109.17/ 90.2 | 109.47 | 106.39 / 92.20 |
| Atomic positions | B (4a) 0, 0, 0<br>P (4c) ¼, ¼ , ¼ | B (3c) ½, 0, 0<br>P (3d) ½, 0, ½ | Al (4a) 0, 0, 0<br>P (4c) ¼, ¼ , ¼ | Al (3c) ½, 0, 0<br>P (3d) ½, 0, ½ |
| $E_{total}$, eV<br>$E_{total}$/FU, eV | -51.59<br>-12.89 | -35.73<br>-11.91<br>ΔE/FU = -0.98 eV | -41.47<br>-10.36 | -29.80<br>-9.94<br>ΔE/FU = -0.427 eV |

Table 2. Elastic constants $C_{ij}$ of BP and AlP polymorphs and **qtz** $C_6$. Bulk ($B_V$), shear ($G_V$) and Young's ($E_V$) moduli calculated by the Voight averaging. All values are in GPa.

| | $C_{11}$ | $C_{12}$ | $C_{13}$ | $C_{33}$ | $C_{44}$ | $C_{66}$ | $B_V$ | $G_V$ | $E_V$ |
|---|---|---|---|---|---|---|---|---|---|
| **qtz** $C_6$ [27] | 1186 | 88 | 64 | 1162 | 549 | 517 | 441 | 550 | 1165 |
| *zb*-BP | 336 | 77 | 77 | 336 | 180 | 180 | 163 | 160 | 362 |
| **qtz** BP | 417 | 45 | 62 | 380 | 186 | 199 | 172 | 186 | 411 |
| *zb*-AlP | 125 | 63 | 63 | 125 | 58 | 58 | 84 | 46 | 117 |
| *NiAs*-AlP | 166 | 81 | 68 | 166 | 42 | 46 | 106 | 47 | 123 |
| **qtz** AlP | 158 | 51 | 60 | 175 | 53 | 52 | 93 | 53 | 133 |

Table 3. Lattice parameters, density (ρ) and Vickers hardness ($H_V$) of BP and AlP polymorphs

| | Space group | $a = b$ (Å) | $c$ (Å) | ρ (g/cm$^3$) | $H_V$ (GPa) | |
|---|---|---|---|---|---|---|
| | | | | | T † | MO ‡ |
| *zb*-BP #216 | *F*-43*m* | 4.5410 | | 2.964 | 30 | 28 |
| **qtz** BP #180 | $P6_222$ | 3.2739 | 3.211 | 3.211 | 33 | 34 |
| *zb*-AlP #216 | *F*-43*m* | 5.4625 | | 2.362 | 10 | 6 |
| *NiAs*-AlP #194 | $P6_3/mmc$ | 3.6084 | 2.967 | 2.967 | 8 | 6 |
| **qtz** AlP #180 | $P6_222$ | 3.8535 | 2.595 | 2.595 | 11 | 6 |

† Thermodynamic model [32]

‡ Mazhnik-Oganov model [21]

**Table 4.** Calculated and experimental properties of BP and AlP polymorphs: bulk moduli ($B_0$) and their first pressure derivatives ($B_0'$); total energies ($E_0$) and volumes ($V_0$) per formula unit; *zb*-to-**qtz** transition pressures ($p_{tr}$) and reduced volumes ($V_{tr}/V_0$)

| | BP | | | AlP | | |
|---|---|---|---|---|---|---|
| | *zb* | | **qtz** | *zb* | | **qtz** |
| | calc. | exp. | calc. | calc. | exp. | calc. |
| $B_0$ (GPa) | 158 | 174(2) [37] | 165 | 83 | 88 [38] | 86.0 |
| $B_0'$ | 3.89 | 3.2(2) [37] | 4.0 | 3.86 | 4 [38] | 4.07 |
| $E_0$/FU (eV) | -12.90 | – | -11.89 | -10.37 | – | -9.92 |
| $V_0$/FU (Å$^3$) | 23.41 | 23.36 [28] | 21.61 | 41.63 | 40.75 [29] | 37.08 |
| $V_{tr}/V_0$ | 0.67 | – | – | 0.81 | – | – |
| $p_{tr}$ (GPa) | 144 | – | – | 28 | – | – |

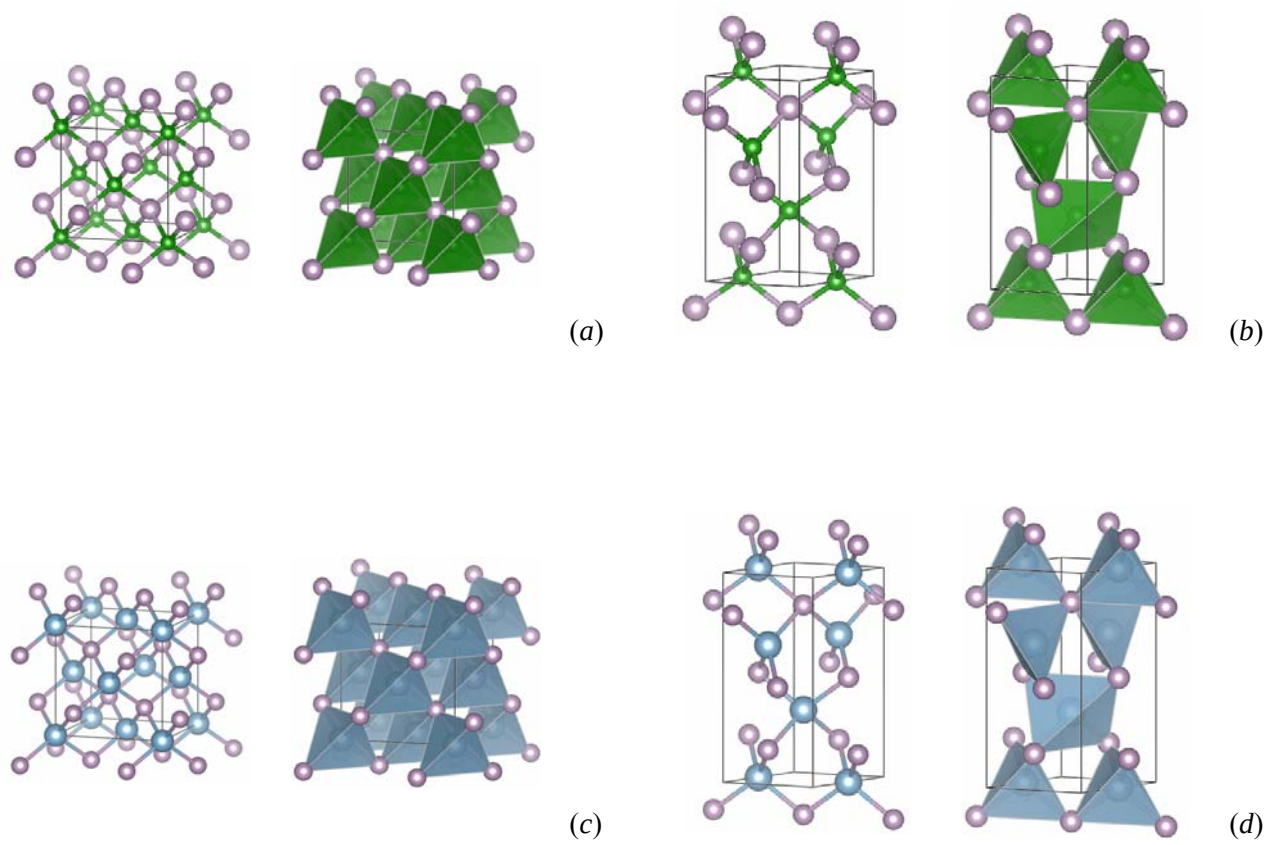


**Figure 1**. Ball-and-stick and tetrahedral representations of cubic (zinc-blende) and hexagonal (**qtz**) structures: (*a*) *zb*-BP; (*b*) **qtz** BP; (*c*) *zb*-AlP; (*d*) **qtz** AlP. Green, blue and purple balls correspond to B, Al and P atoms, respectively.

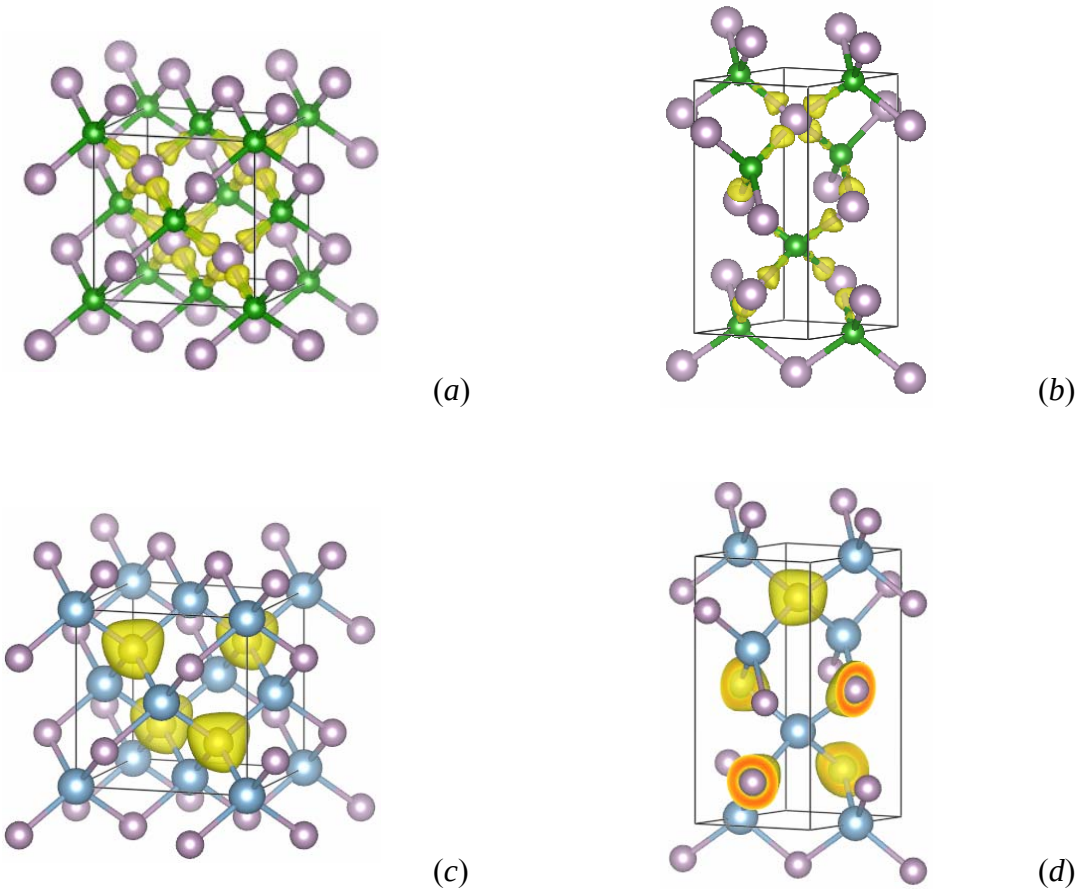


**Figure 2**. Charge density projections of *zb*-BP (*a*); **qtz** BP (*b*); *zb*-AlP (*c*); and **qtz** AlP (*d*). Green, blue, and purple spheres correspond to B, Al, and P atoms, respectively. The *c*-axis along the vertical direction.

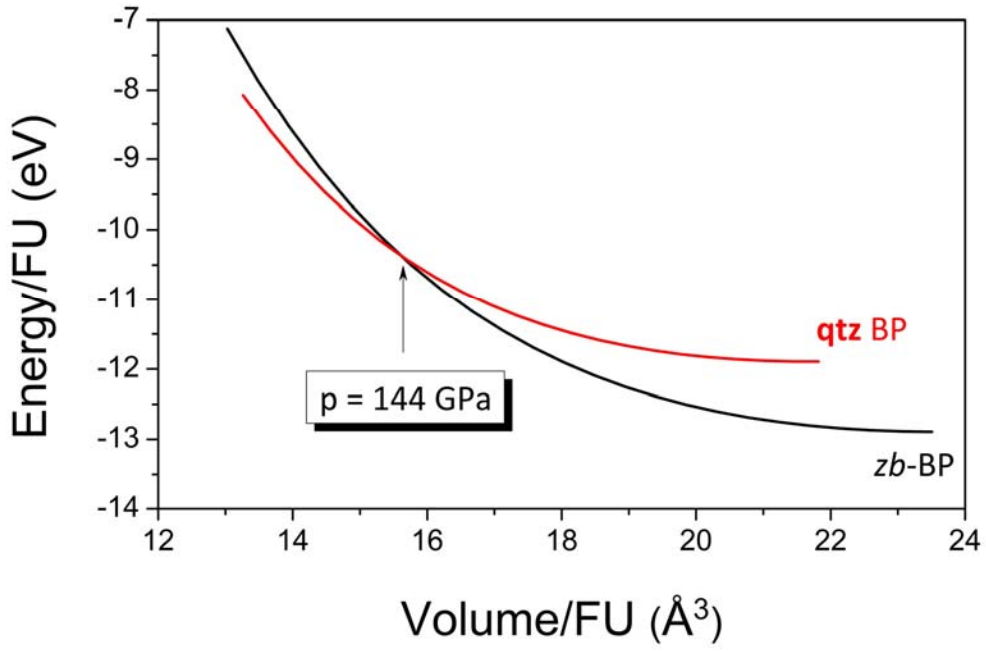


(*a*)

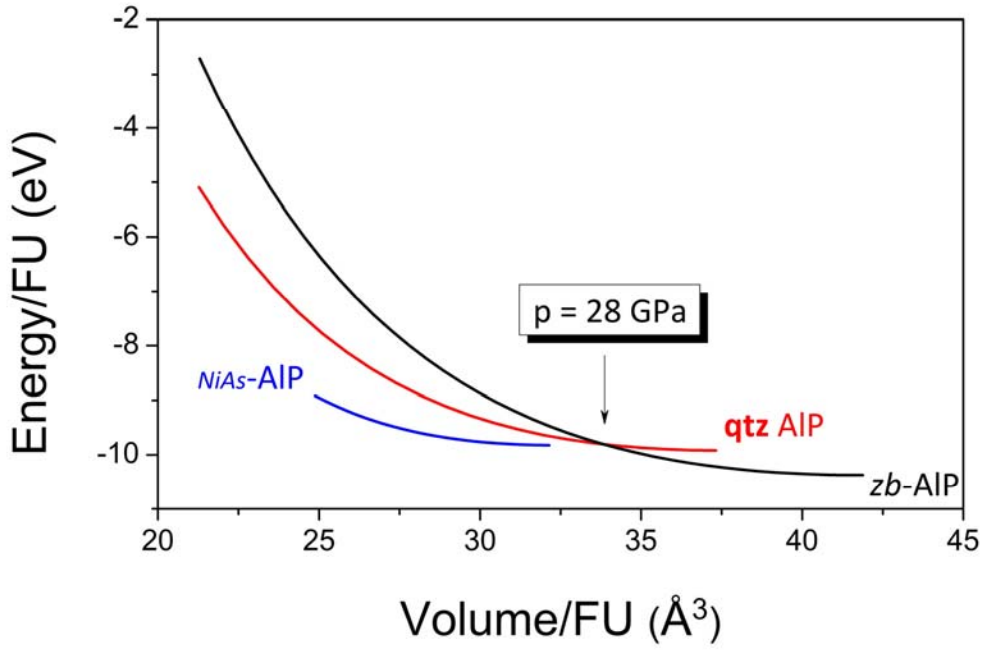


(*b*)

**Figure 3.** Calculated total energies per formula unit as function of volume for BP (*a*) and A1P (*b*).

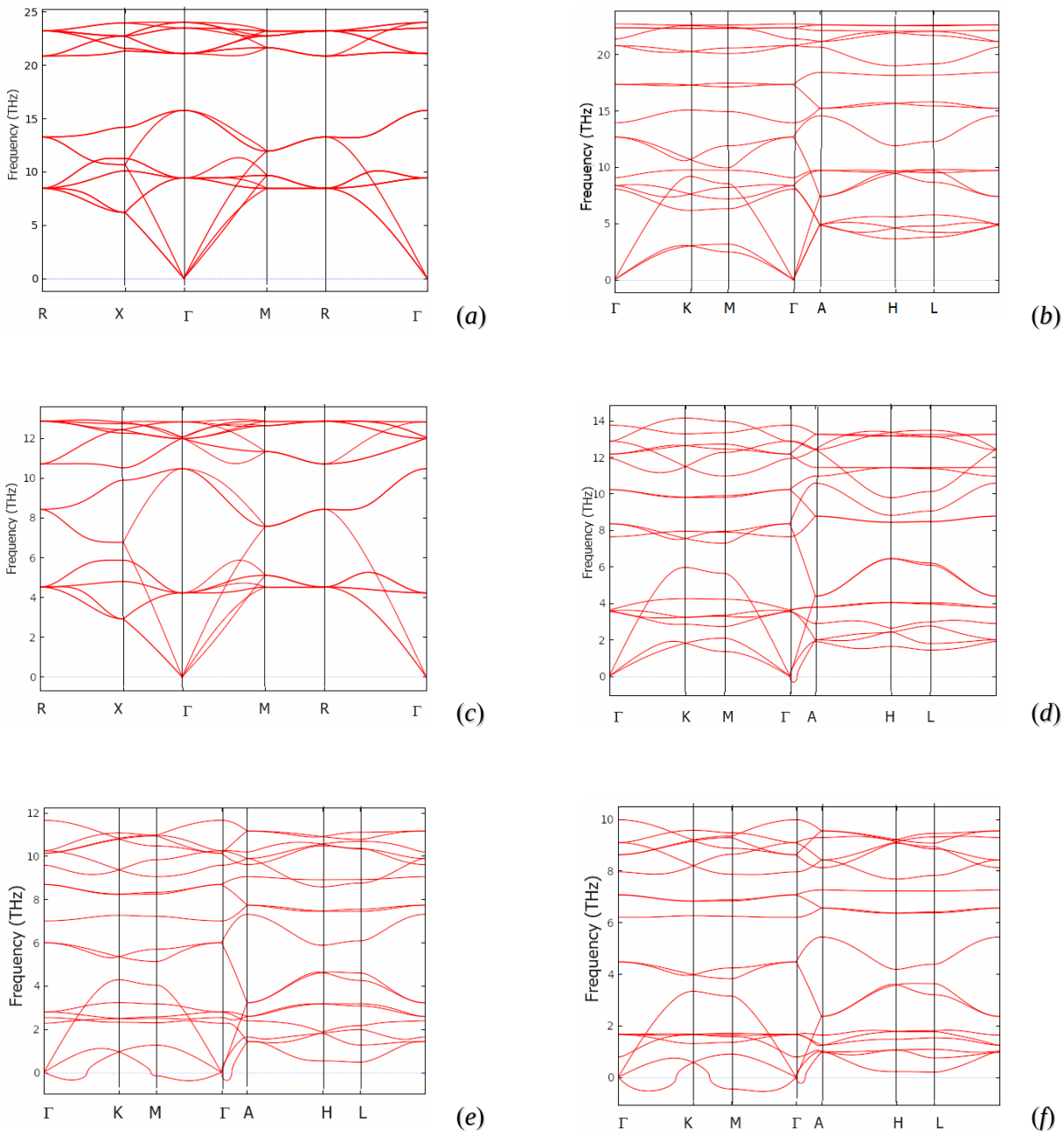


**Figure 4**. Phonon band structures of *zb*-BP (*a*); **qtz** BP (*b*); *zb*-AlP (*c*); **qtz** AlP (*d*), **qtz** GaP (*e*) and **qtz** IP (*f*).

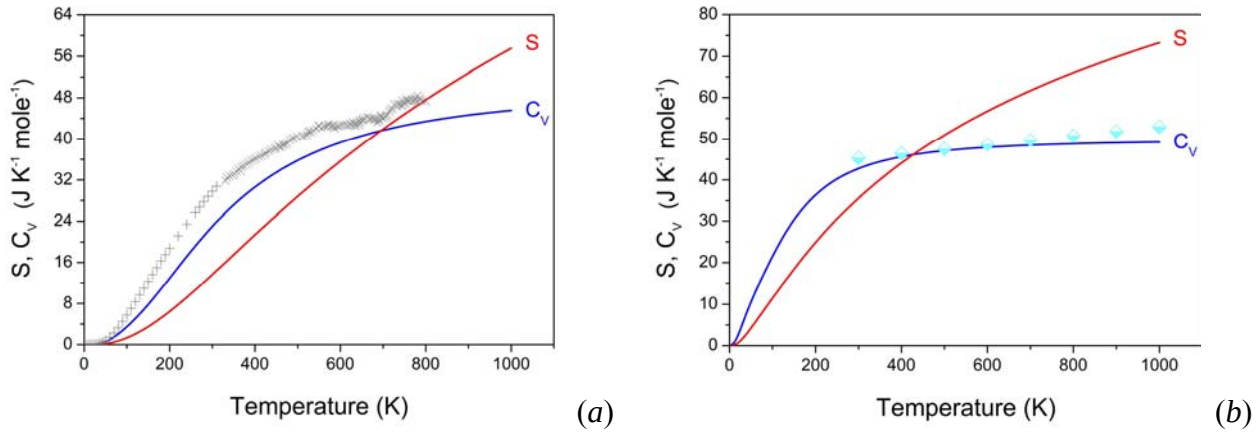


**Figure 5**. Heat capacity at constant volume ($C_V$) and entropy (S) of **qtz** BP (*a*) and **qtz** AlP (*b*) as functions of temperature. Experimental heat capacity data for *zb*-BP [43,44] and *zb*-AlP [45] are shown as gray and cyan symbols, respectively.

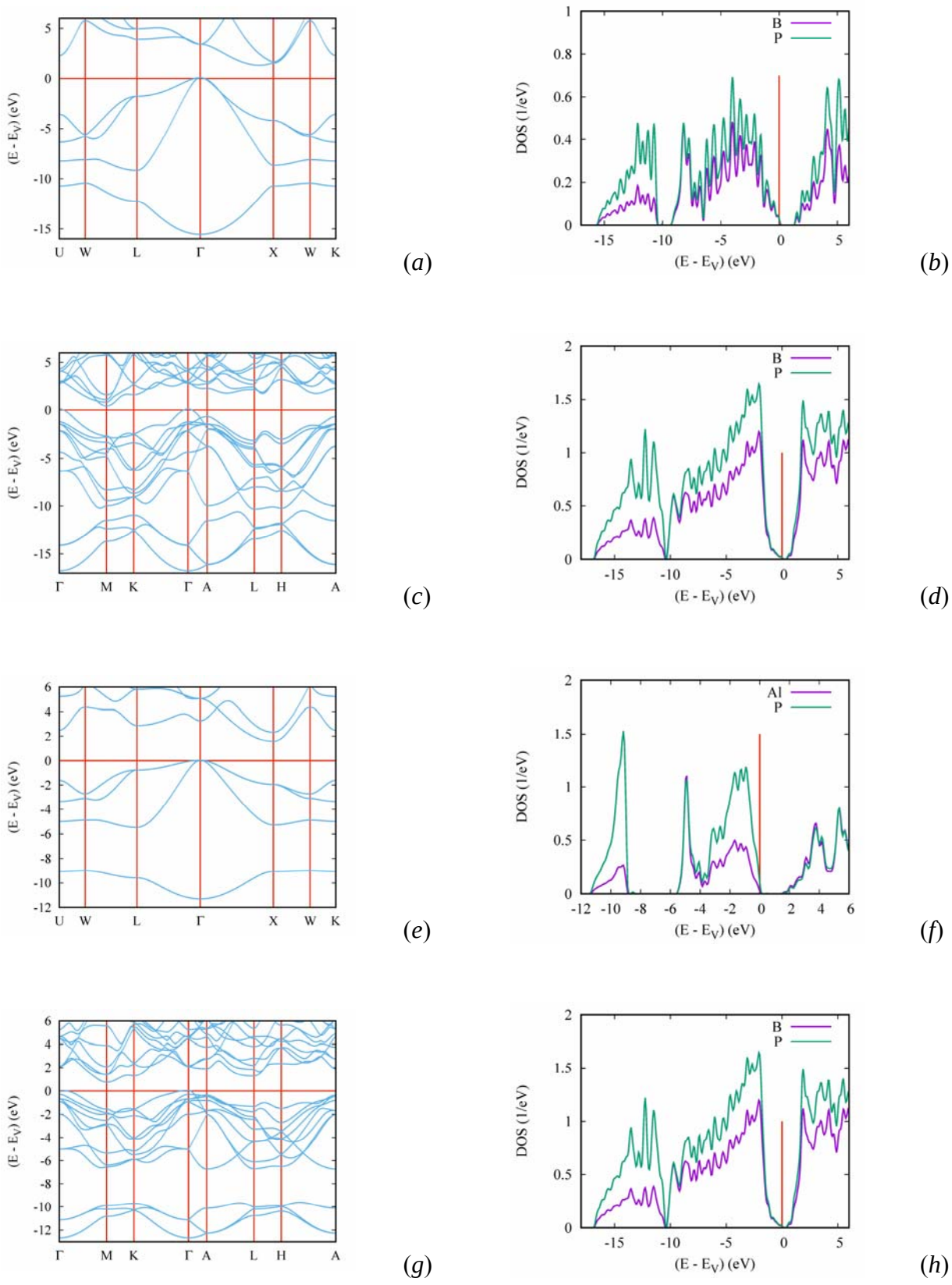


**Figure 6**. Electronic band structures (left) and site projected density of states (right) of *zb*-BP (*a*,*b*); **qtz** BP (*c*,*d*); *zb*-AlP (*e*,*f*); and **qtz** AlP (*g*,*h*).